# Chronic Lead Exposure Causes Theta and Gamma Hypersynchrony in the Hippocampus and Disrupts Sensorimotor Gating

Abbreviated Title: LEAD EXPOSURE CAUSES HIPPOCAMPAL HYPERSYNCHRONY

Nathan W. Schultheiss[1], Jennifer L. McGlothan[2], Tomás R. Guilarte[2*], Timothy A. Allen[1,2,3*]

[1]Department of Psychology, Florida International University, Miami, FL, 33199
[2]Department of Environmental Health Sciences, Robert Stempel College of Public Health, Florida International University, Miami, FL, 33199
[3]Cognitive Neuroscience Program, Florida International University, Miami, FL, 33199

Number of figures: 8
Number of supplemental figures: 1
Number of tables: 1
Number of text pages: 33
Total character count (with spaces):
Title: 111
Abstract: 1,847
Introduction: 5,678
Methods: 16,253
Results: 12,809
Discussion: 5,924
References: 9,792
Total: 59,514

*Corresponding Authors:

Timothy A. Allen, PhD
Department of Psychology
email: tallen@fiu.edu
Website: http://allenlab.fiu.edu/
Twitter: @AllenNeuroLab

Tomás R. Guilarte, PhD
Department of Environmental Health Sciences
email: tguilart@fiu.edu
website: https://stempel.fiu.edu/brain-behavior-environment-laboratory/
Twitter: @guilartelab

Address:
Florida International University
11200 SW 8th Street
Miami, FL, 33199

Conflict of Interest: The authors declare no competing financial interests.
Acknowledgements: This work was supported by R01 ES006189 to T.R.G. and R01 MH113626 to T.A.A.
Keywords: hippocampus, schizophrenia, lead neurotoxicity, pre-pulse inhibition

## ABSTRACT

Chronic lead ($Pb^{2+}$) exposure from childhood contributes to an array of cognitive and behavioral dysfunctions including impaired attention and intellectual ability, learning and memory deficits, and delinquency. It is also an environmental risk factor for adult psychopathologies, most notably schizophrenia. $Pb^{2+}$ is a potent N-methyl-D-aspartate receptor (NMDAR) antagonist and exposure during early life elicits a cascade of cellular neurotoxic effects that alter the developmental trajectory leading to a loss of parvalbumin-expressing interneurons in hippocampus and altered synaptic transmission. Little is known, however, about the impact of chronic $Pb^{2+}$ exposure on hippocampal network dynamics which serve as a link between cellular-molecular effects and cognitive-behavioral consequences of $Pb^{2+}$ neurotoxicity. Here, we tested the effects of chronic $Pb^{2+}$ exposure on local field potential activity (LFP) in the hippocampus of freely-behaving rats. We demonstrate that $Pb^{2+}$ exposure causes striking hypersynchrony in both the theta- and gamma-frequency bands, in addition to more modest changes in delta. Next, we tested the effect of $Pb^{2+}$ exposure on prepulse inhibition of the acoustic startle reflex (PPI) in male and female rats at different developmental timepoints. We found that adult males (PN50 and 120), but neither females nor juvenile males, showed reduced PPI that could not be attributed to changes in the startle reflex. This pattern recapitulates sex- and age-dependencies of PPI disruption in schizophrenic patients. Overall, these results are consistent with the hypothesis that $Pb^{2+}$ is an environmental risk factor for psychopathology in adulthood, especially those symptoms related to cognitive and sensory-motor gating processes that depend on rhythmic coordination of network activity in the hippocampus.

## Introduction

Environmental exposure to lead ($Pb^{2+}$) is a major health problem affecting millions of people worldwide. $Pb^{2+}$ exposure in children has been linked to reduced intellectual abilities, increases in delinquent and antisocial behaviors, and attention deficit and hyperactivity disorder (Needleman et al., 2002; 2004; Miranda et al., 2007; Canfield et al., 2003; Caito & Aschner, 2017). Further, early life $Pb^{2+}$ exposure has been proposed as an environmental risk factor for adult psychopathology, most notably with regard to schizophrenia (Opler et al., 2004; 2008). A current leading hypothesis is that schizophrenia is best understood as the result of interactions between genetic and environmental factors (Guilarte et al., 2012), with evidence that $Pb^{2+}$ exposure exacerbates cognitive and behavioral deficits in the DISC1 knock out mouse model of schizophrenia (Abazyan et al., 2014).

Understanding the relationship between $Pb^{2+}$-exposure and mental health pathologies requires a neurobiological approach to establishing the link between genetic and environmental factors. At the cellular and molecular levels, much is known about $Pb^{2+}$ effects on the developing brain. $Pb^{2+}$ is a potent N-methyl-D-aspartate (NMDA) receptor antagonist (Guilarte, 1997; Guilarte & Miceli, 1993; Guilarte & Miceli, 1992). Low-to-moderate $Pb^{2+}$ levels in the brain (which has no endogenous function) leads to NMDAR hypoactivity, which can alter the developmental trajectory of the NMDAR subunits (Guilarte & McGlothan, 1998; Nihei et al., 2000), and impair the maintenance synaptic long-term potentiation (Nihei et al., 2000). At the cellular level, $Pb^{2+}$ exposure causes a reduction in the number of parvalbumin-labeled GABAergic interneurons in the hippocampus and agranular medial prefrontal cortex (Stansfield et al., 2015), a hallmark cellular pathology in schizophrenic brains (e.g., Hashimoto et al., 2003). At the level of the whole brain, annual childhood blood $Pb^{2+}$ levels have been found to be inversely correlated with cortical gray matter volume (Brubaker et al., 2010). Likewise, an electroencephalography (EEG) study of $Pb^{2+}$-exposure, as measured by tooth $Pb^{2+}$, showed there are significant alterations in delta, theta and gamma bands related to cognitive function, the severity of which corresponded to the exposure levels (Needleman, 1983).

However, the bridge between the cellular-molecular and cognitive-behavioral levels is not well understood. Linking these levels requires animal models of $Pb^{2+}$ exposure allowing for invasive techniques that can establish a causal link between $Pb^{2+}$ exposure, specific neurobiological mechanisms, and

behaviorally-relevant network consequences. Here, we performed chronic *in vivo* hippocampal recordings from a well-established rodent model of $Pb^{2+}$ exposure during open field behaviors (Schultheiss et al., 2020). This initial study of the rhythmic network effects of chronic $Pb^{2+}$ exposure focused on the hippocampus because chronic $Pb^{2+}$-exposure causes reliable and severe deficits in hippocampal-dependent spatial learning (Kuhlmann et al., 1997; Jett et al., 199; Munoz et al., 1988) which can be ameliorated with environment enrichment (Cao et al., 2008; Guilarte et al., 2002), similar to other hippocampal insults. Likewise, $Pb^{2+}$-exposure causes contextual but not cued fear conditioning deficits (Jaako-Movits et al., 2005; McGlothan et al., 2008; Wang et al., 2016), in addition to fear extinction impairments (McGlothan et al., 2008). These behavioral results are consistent with the central role of hippocampal networks in mediating the effects of chronic $Pb^{2+}$-exposure in psychotic disorders.

Our recordings and analysis focused on the spectral content of local field potentials (LFPs) from the hippocampus in of $Pb^{2+}$-exposed rats using multisite silicon probes during stationary and running behaviors. LFPs are a good choice to examine network properties because they reflect the rhythmic synchrony among neurons aggregating local and long-range synaptic potentials. We observed several key abnormalities, most notably excessive hypersynchrony in the theta and gamma bands and abnormal behavior-related changes the theta and gamma bands. Hypersynchrony is detrimental to local network processing and has been observed in other disorders. For example, hippocampal hypersynchrony in the theta and slow gamma ranges have also been observed in the LFP recordings of the freely-behaving *Fmr1-KO* mouse, a genetic model of Fragile X syndrome which is characterized by intellectual disability (Arbab et al., 2018).

Next, because over activation of the hippocampus is known to cause impaired sensory-motor gating (Bast et al., 2001a,b; Bast et al. 2003), we followed the network finding up by looking at the consequences of Pb2+-exposure on prepulse inhibition of the startle reflex (PPI). We found that $Pb^{2+}$-exposure caused large and reliable sensory-motor gating deficits in male, but not female, adult rats in developmentally-relevant pattern (PN50 and PN120, but not PN28). These effects could not be attributed to baseline startle levels, and are in line with the $Pb^{2+}$ hypothesis of schizophrenia because PPI impairments are a hallmark pathological phenotype in the disease.

Altogether the present findings show that $Pb^{2+}$ exposure leads to pathological theta and gamma hypersynchrony in the hippocampus and causes sensory-motor gating deficits. These abnormal hippocampal network effects may explain both the cognitive and the sensory-motor gating deficits seen in adult psychopathologies resultant of Pb2+ exposure, and suggests targeting hippocampal network restoration as a therapeutic target.

## Methods

*Subjects.* Nine adult male Long-Evans rats were used in electrophysiological experiments. Five of these were chronically exposed to lead ($Pb^{2+}$), and four were controls. Two hundred thirty rats were used in PPI experiments. These rats were evenly divided into twelve groups (18-21 per group) corresponding to all combinations of (1) $Pb^{2+}$ exposure and controls, (2) males and females, and (3) three ages at the time of testing. All rats were individually housed in a climate-controlled vivarium on a reversed 12hr light/dark cycle, and experiments were conducted during the dark cycle active periods. Rats had free access to food and water when in their home cages, but no food or rewards were available during behavioral sessions. All studies were carried out in strict accordance with the recommendations in the Guide for the Care and Use of Laboratory Animals of the National Institutes of Health under protocols approved by Florida International University Institutional Animal Care and Use Committee. Data from the four control rats in the electrophysiological experiments were previously analyzed to establish the relationships of hippocampal spectral modes to behaviors (Schultheiss et al., 2020). The present study focuses on the effects of $Pb^{2+}$ exposure and all analyses presented here are new.

*Breeding and Chronic $Pb^{2+}$ Exposure.* Prior to breeding, adult female rats (225-250 g) were purchased from Charles River Laboratories and randomly assigned to a Prolab RMH-1000 diet containing 0 (control) or 1500 ppm lead acetate (PbAc) (Dyets, Inc., Bethlehem, PA). After 10-14 days of acclimation to the diet, each dam was paired with a non-exposed adult male Long Evans rat (250-275 g; Charles River Laboratories) to breed over 3 days. Litters were culled to 10 pups on postnatal day one (PN1). Dams were maintained on their respective diet, and at PN21 male pups were weaned onto the same diet and maintained for the duration of the experiments.

*Silicon probe implants.* All electrophysiological procedures were the same as we have previously described (see Schultheiss et al., 2020 for details). Briefly, silicon probes with 32 recording electrodes arranged as eight tetrodes were surgically implanted for recording local field potentials (LFPs) from dorsal hippocampus (HC). The eight tetrodes were distributed across four shanks of the probe at tip-to-tetrode depths of 78 μm and 228 μm (NeuroNexus A4X2-tet-5mm). Shanks were separated by 200 μm giving each probe a total length of 0.67 cm which was oriented medial-lateral when implanted to sample along the proximal-distal axis of the CA1 subregion of HC. Electrode impedances were 1.23 ± 0.32 MΩ.

*Surgical procedures.* The rats used in electrophysiological experiments weighed 600-700 g at the time of surgery. General anesthesia was induced with isoflurane (5%) mixed with oxygen (0.8 L/min) that was continuously delivered throughout surgery at 1-4% as needed. Body temperature was monitored throughout surgery, and a Ringer's solution (5% dextrose) was given periodically to maintain hydration (1 ml increments every 60-90 minutes). Once the hair over the scalp was cut, rats were placed in a stereotaxic device, and glycopyrrolate (0.5 mg/kg, s.c.) was administered to assist respiratory stability. Ophthalmic ointment was then applied to the eyes. Four injections of marcaine were made to the scalp (~0.1 ml, 7.5 mg/ml, s.c.), and a rostrocaudal incision was made exposing the skull. The pitch of the skull was leveled between bregma and lambda, two stainless steel ground screws were placed in the left parietal bone, and five titanium support screws were anchored to the skull. Rectangular craniotomies were drilled to accommodate the probe shanks centered on coordinates A/P -3.24 mm, M/L 2.7 mm. After removal of the dura, the probe was lowered on the stereotaxic arm until the tips of the probe shanks were just above the cortical surface. Then, the ground wire was attached to the ground screws, and implants were lowered further until the electrodes reached a depth of ~2.8 mm below the cortical surface. A thin layer of sodium alginate was applied in the craniotomy to protect the exposed surface of the brain, and dental cement was applied to permanently secure the implant to the skull screws. Neosporin® was applied to the skin surrounding the implant, and flunixin (2.5 mg/kg, s.c.) was given for analgesia. Following surgery, rats were allowed to rest on a heating pad until ambulatory, prior to being returned to their home cages. Neosporin® and flunixin were given again on the day following surgery, and rats were monitored closely for five days to ensure that body weight was maintained. Daily Baytril injections (s.c.) were also

given for five days to protect against postsurgical infection. A minimum of one week was reserved for recovery prior to beginning experiments.

*Behavioral Setup.* All electrophysiological experiments were conducted in a large open field environment (122 x 118 x 47 cm). A custom-made white cutting board served as the floor of the behavioral arena, and the interior walls were lined with white vinyl. The arena was mounted on stilts 72 cm above the floor and the exterior was wrapped in grounded Faraday shielding. Two video cameras were used for behavioral tracking with a bird's eye view. These were mounted 28 cm apart from one another,150 cm above of the arena floor, providing ~4.6 pixel/cm resolution in recorded videos and corresponding tracking data.

The entire behavioral apparatus was enshrouded with black curtains suspended from the ceiling and extending to the floor. Small gaps at the Velcro® closures between the four curtain panels were used to observe rats covertly to monitor that the head-stage, cables, and elastic tethers were not tangled, and to confirm that rats were awake during periods of relative inactivity. All room lights were kept off during recording sessions, and the white arena was illuminated dimly with red light from LED strips mounted above at the level of the video cameras.

During behavioral sessions rats were placed on the arena floor and recorded without any intervention except for infrequent behavioral checks or to adjust cables or connections.

*Electrophysiological recordings.* Throughout each experiment wide-band neural data were acquired with a Plexon OmniplexD recording system with A/D conversion at 40 kHz (16 bit). A digital head stage processing subsystem (Intan, 32 channel) passed continuous wide-band data referenced against the ground screws (low cutoff = 0.7 Hz) to a hard drive using PlexControl data acquisition software. For analysis of LFP recordings, wideband data was down-sampled to 2 kHz. A maximum of one channel per tetrode was included in our analyses, and twelve tetrodes were excluded for poor signal. As a result of these restrictions, 30 channels recorded from $Pb^{2+}$-exposed rats were analyzed, and 30 channels from control animals were analyzed. All of the selected channels were included in all analyses, providing a robust sampling of hippocampal recording sites for each group.

*Behavioral tracking.* The physical and software settings for the two video cameras used for behavioral tracking were tuned independently to optimize detection of body contours on one camera and to optimize tracking of head-mounted LEDs on the other. LED tracking entailed tabulating the coordinates of two clusters of LED florets (one green and one blue) that were offset ~2 cm laterally from the head-stage at ~3 cm above the rat's head. Each LED cluster comprised three florets oriented upward and slightly outward. This construction enabled consistent LED tracking despite behaviors in which rats oriented their heads away from the level plane. Body location was calculated from difference images obtained by subtracting an image of the empty arena from each frame capture during an experiment. Movement speeds were calculated from these body coordinates. The location of the head was calculated as the midpoint between the two LED clusters for each timepoint. Using Cineplex software (Plexon), LED tracking data was collected online during experiments, and body contour tracking was derived offline from recorded videos. Video tracking frame captures (30 fps) were synchronized in real time to the simultaneously recorded neural data via a central timing board (Plexon).

*Co-registration of LED and body tracking data.* Following acquisition, all analyses of behavioral data were performed with custom-written Matlab scripts (MathWorks, Natick, MA). First, the coordinate system for camera one was mapped onto the coordinate system for camera two, enabling integration of the two types of tracking data. We then derived for each timestep the animal's head direction (HD) relative to the environment (from the axis between the two head-mounted LED clusters); body direction (BD) relative to the environment (from the midpoint between the LEDs to the center of the body); head angle (HA) relative to the body (using the LED axis relative to BD); and the rotational velocity of the body.

*Definitions of running and stationary bouts.* Rats exhibit a wide range of behaviors that involve body and head movements at substantial speeds. These movements appear in tracking data as changes in body and LED coordinates, just as running does. To isolate bouts of locomotion from other behaviors including grooming and rearing, we first required that movement speed be maintained above 5 cm/sec for a minimum duration of 1.025 or 2.05 seconds with a minimum peak speed of 15 cm/sec. We then eliminated all instances where head angle exceeded 35 degrees or body rotational velocity exceeded 52.5 degrees

per second at any time. Stationary bouts were required to meet the same minimum duration, HA, and rotational criteria and not exceed a maximum movement speed of 5 cm/sec.

*Derivation of oscillatory metrics.* We evaluated the correspondence to animals' movement speeds of LFP dynamics in the delta-, theta-, and slow and fast gamma-frequency bands (1-4 Hz, 6-10 Hz, 25-55 Hz, and 65-120 Hz, respectively) using amplitude timeseries for each band and using the power spectral density of the LFP. We derived amplitude timeseries for each band by resampling to 2kHz the peak-to-trough amplitudes of each oscillatory cycle of the respective band-pass filtered LFPs. The spectral content of HC recordings was estimated using Welch's method for each stationary and running bout. The 1.025 and 2.05 second minimum durations required in our bout definitions were chosen as a compromise between the relatively fast timescale of rats' locomotor behaviors, e.g. bouts of running and interspersed pauses, and the reduction in number of oscillatory cycles (particularly for delta) contributing to amplitude measures for shorter time windows.

Estimates of delta and theta power from the PSDs for individual behavioral bouts were defined as the mean values across the respective frequency ranges. For each recording site, delta and theta power estimates were defined as the medians of these values across all bouts of each type. The distributions of these values for each group are plotted as insets in Figure 3.

Delta and theta peak frequencies and peak power estimates were measured directly from the PSDs for behavioral bouts. Scatterplots of these values are shown in Figure 4. Correlation coefficients relating these measures to running speed were derived for each recording site across all bouts of each type. Distributions of these correlation coefficients for each group are shown in Figure 5.

We defined behavioral modulation of oscillatory metrics as the difference between running bouts and stationary bouts. First, mean PSDs across bouts of each type were derived for each recording site. Then behavioral modulation was calculated for each site as the subtraction of the mean stationary PSD from the mean running PSD. Behavioral modulation for each site was then normalized either by the area of the mean stationary PSD (as in Figure 6A) or by dividing by the mean stationary PSD to give the percent change at each frequency (as in Figure 6B). Behavioral modulation of delta and theta were then defined as

the mean values across the respective bands for each recording site. Distributions of these values are shown as scatterplots in Figure 6.

To further evaluate the effects of $Pb^{2+}$ exposure on oscillatory synchronization in each frequency band, we collected peak-to-trough amplitude measurements for every cycle of band-pass filtered LFPs for each recording site for all bouts of each type. The normalized distributions of these amplitude measurements are plotted in Figure 7.

*PPI experiments*. Pre-pulse inhibition of acoustic startle (PPI) was assessed in male and female rats at PN28, PN50, and PN120 following a protocol adapted from Abazyan et al. (2014). Four identical SR-LAB startle chambers (San Diego Instruments Inc., San Diego, CA, USA) were used to measure startle responses. Rats were placed inside the startle chamber into a mounted Plexiglas® cylinder with an accelerometer. Broadband background noise and acoustic stimuli were delivered via a speaker on the ceiling of the chamber. Sound levels were calibrated using a digital sound level meter, and accelerometer sensitivities for each chamber were calibrated daily. Presentation of acoustic stimuli was controlled by the SR-LAB software and interface system, and accelerometer measurements were recorded. Each experimental session started with a five-minute period during which rats acclimatized to 68 dB background noise that was continuous throughout the session. Next, rats' average startle responses were calculated as the mean of 10 acoustic pulses (120dB, 100ms) presented at a random inter-trial intervals. Rats were left in the enclosure for an additional five minutes prior to beginning PPI trials. Rats were exposed to the following trial types: pulse-alone trial (120dB, 100ms); pre-pulse alone (90dB, 20ms); and four pre-pulse–pulse combinations (20 ms pre-pulse presented 80 ms before the 120 dB, 100 ms pulse) using one of the five pre-pulse intensities: 74, 78, 82, 86 and 90 dB. Each session consisted of six presentations of each trial type presented in a pseudorandom order with random inter-trial intervals. The average response during the 100 ms recording window beginning at stimulus onset was used as the measure of startle responses. PPI was quantified for each animal as the percent change in startle amplitude on pre-pulse–pulse trials relative to pulse-alone trials.

*Blood $Pb^{2+}$ Levels.* Blood $Pb^{2+}$ levels of rats used in PPI experiments (Table 1) were measured in samples obtained from cardiac puncture under sodium pentobarbital anesthesia. Samples were prepared

295 and measured following protocols provided using the LeadCare Plus system (Magellan Diagnostics, N.
296 Billerica, MA).

297 *Histology.* At the completion of data collection, rats used in electrophysiological experiments were
298 anesthetized with isoflurane (5%) mixed with oxygen (800 ml/min) and marking lesions were made with a
299 NanoZ (Plexon) to deliver 10μA for 10s at each electrode locations. About an hour later, rats were
300 transcardially perfused with 100 ml phosphate-buffered saline (PBS), followed by 200 ml of 4%
301 paraformaldehyde (PFA, pH 7.4; Sigma-Aldrich, St. Louis, MO). Blood $Pb^{2+}$ levels of these rats were
302 measured in samples obtained from cardiac puncture during the perfusion. Brains were post-fixed
303 overnight in 4% PFA and then placed in a 30% sucrose solution for cryoprotection. Frozen brains were cut
304 on a Leica CM3050 S cryostat (40 μm; coronal) and Nissl-stained. Marking lesions were mapped onto
305 plates of the Paxinos & Watson Atlas (2004).

306

307 **Results**

308 Our analyses focused on relationships between locomotor behaviors and concurrent hippocampal
309 synchronization in delta-, theta-, and gamma-frequency bands to assess the impact of $Pb^{2+}$ exposure on
310 network dynamics in hippocampus and possible commonalities with the pathophysiology of schizophrenia.
311 For this we compared the spectral content of local field potential (LFP) recordings from hippocampus
312 (Figure 1A&B) in rats chronically exposed to $Pb^{2+}$ and controls.

313 *Overall Behavior*. Recordings were made throughout behavioral sessions during which rats freely
314 explored a large 'open field' arena (122 cm x 118 cm). No task was imposed during behavioral sessions; no
315 rewards were delivered; and environmental stimuli and experimenter contact were strictly minimized. Under
316 these conditions, we did not observe any differences between $Pb^{2+}$-exposed rats and controls in
317 continuous behavioral measures including movement speed, spatial orientation, and rotation velocity
318 (Supplemental Figure 1). Rats in both groups were more often stationary (~20-40% of session time) than
319 moving at any other speed, but all rats exhibited sporadic episodes of exploration yielding a consistent
320 peak in speed occupancy at ~7 cm/s. These active episodes typically comprised running, rearing, and
321 olfactory sampling behaviors, and were interspersed amongst periods of grooming and awake inactivity. To

322 sharpen our analysis, we isolated precisely-defined bouts of running and stationary behaviors, and
323 excluded rearing, grooming, and reorienting behaviors by imposing exclusion thresholds for speed,
324 rotation, and head angle as in Schultheiss et al. (2020). Bout-wise measures of running and stationary
325 behavior were also equivalent between $Pb^{2+}$-exposed rats and controls (Supplemental Figure 1D and 1E).

326 *Movement speed modulation of delta, theta, and gamma oscillations.* To provide initial insight into
327 relationships between neural rhythms and locomotor behavior, we derived instantaneous amplitude
328 timeseries for delta-, theta-, and gamma-frequency bands by resampling peak-to-trough measurements for
329 each cycle of the respective band-pass filtered LFP. The amplitudes of delta, theta, and fast gamma
330 oscillations were all consistently modulated by animals' movement speeds in both control and $Pb^{2+}$-
331 exposed rats (Figure 1C). Whereas theta and gamma were positively correlated to speed, delta was
332 negatively correlated to movement speed (Schultheiss et al., 2020). Figure 1C shows these relationships
333 for all recording sites in all rats (n = 30 per group), illustrating the qualitative similarity between groups.
334 Movement speed modulation of slow gamma amplitude was generally less prominent or absent, but some
335 recording sites in both control and $Pb^{2+}$-exposed animals exhibited negative correlations to speed.

336 As we have recently demonstrated, distinct modes of delta- and theta-dominated hippocampal
337 network activity can transition rapidly in tandem with the stops and starts of rats' locomotor trajectories. In
338 that study delta and theta power were orthogonal across modes such that strong delta synchronization
339 occurred when theta was weak and vice versus. This pattern of exclusivity between hippocampal modes
340 may reflect distinct neurophysiological processes or cognitive functions contributing to spatial navigation
341 and memory (Schultheiss et al., 2020). Thus, to minimize blurring the oscillatory dynamics of distinct
342 modes that accompany behaviors occurring in rapid succession, we focused our subsequent analyses on
343 hippocampal synchronization during the precisely-defined stationary and running bouts.

344 Power spectral densities (PSDs) of the HC LFP showed higher delta power during stationary bouts
345 and higher theta power during running bouts for both $Pb^{2+}$-exposed animals and controls. Figure 2 A and B
346 illustrate representative PSDs for two rats in each group, and show considerable variability across
347 recording sites from individual rats in the delta power exhibited during stationary bouts. Linear fits to delta
348 power across individual recording sites from each rat revealed a consistent distal-proximal gradient of

increasing delta power in control animals that was not evident in $Pb^{2+}$-exposed animals (Fig. 2C). No consistent theta power gradient was observed during running bouts for either group (Fig. 2D).

$Pb^{2+}$-exposed rats exhibited marked elevation of theta power relative to controls during both stationary bouts (1 sec: p=0.01, t=-2.6, df=58; 2 sec: p=0.04, t=-2.1, df=58) (Fig. 3A) and running bouts (1 sec: p=0.002, t=-2.8, df=58; 2 sec: p=0.002, t=-3.2, df=58) (Fig. 3B). Delta power in $Pb^{2+}$-exposed rats was also elevated relative to controls during two second stationary bouts (p=0.05, t=-2.1, df=58), but this trend was weak for one second bouts that are generally more strongly impacted by behavioral variability (p=0.14, t=-1.5, df=58). No differences in delta power between groups were observed during running.

We also found that theta frequency was substantially lower in $Pb^{2+}$-exposed rats compared to controls during both stationary bouts (control: 7.2 ± 1.1, Pb: 6.8 ± 1.0; $p=8.1\times10^{-6}$, t=-4.5, df=842) and running bouts (control: 8.2 ± 0.4, Pb: 7.8 ± 0.6; $p=3.9\times10^{-25}$, t=-10.77, df=702) (Fig.4A). Interestingly, pairwise 2-D scatterplots of theta power, theta frequency, and running speed for each bout type suggest that (1) covariation of theta power and theta frequency was disrupted in $Pb^{2+}$-exposed rats relative to controls (Fig. 4A, right; green vs black lines); and (2) running speed modulation of theta frequency was confined to a narrower range of speeds (Fig. 4B, right; green vs black lines); and in contrast, (3) running speed modulation of theta power occupied similar parameter spaces in $Pb^{2+}$-exposed rats and controls (Fig. 4C, right; green vs black lines). Taken together, these observations suggest that $Pb^{2+}$ exposure may disrupt the fidelity of relationships between theta synchronization and locomotor behavior. To evaluate this quantitatively, we focused on two second running bouts and compared distributions across recording sites of the correlation coefficients between running speed and theta (and delta) measures. As expected, we found positive correlations of theta power and frequency to running speed for the majority of recording sites in both $Pb^{2+}$-exposed rats and controls (Fig. 5). Importantly, we also found that the fidelity of theta power to running speed was heightened in $Pb^{2+}$-exposed rats relative to controls (p=0.0149, t=2.511, df=58), potentially reflecting a reduction in the dimensionality of hippocampal representations in favor of locomotor parameters, i.e. limiting the integration of multidimensional information arriving at the hippocampus from widespread cortical regions. However, in contrast to the apparent restriction of running speed modulation of theta frequency to a narrower range of speeds in $Pb^{2+}$-exposed rats (Fig. 4B), we found that correlations

between running speed and theta frequency were similar in strength between groups (Fig. 5C, top vs bottom; p=0.192, t=-1.319, df=58).

Interestingly, delta power was unrelated or even positively correlated to running speed in control animals across running bouts, but it was significantly negatively correlated to running speed in $Pb^{2+}$exposed rats. Accordingly, comparison of running speed modulation of delta power showed a significantly strengthened negative correlation in $Pb^{2+}$exposed rats (delta power, p=0.0026, t=3.143, df=58). It is important to consider, however, that these correlations of delta parameters to running speed were taken across running bouts when delta is often weak or absent. As a result, they may reflect theta-delta interactions that are distinct from the differences between delta- and theta-dominated modes that parallel behavioral state changes.

Next, we evaluated differences in behavioral modulation of the PSD between $Pb^{2+}$-exposed rats and controls by subtracting mean PSDs for stationary bouts (normalized by the integral of the PSD) from the corresponding mean PSDs for running bouts for each recording site. This approach yielded 'difference spectra' that revealed stronger behavioral modulation of theta and the first harmonic of theta in $Pb^{2+}$-exposed animals relative to controls (Fig. 7A). Augmentation of the difference in theta synchronization between behavioral states may reflect increased susceptibility of HC to entrainment by theta rhythmic inputs recruited during running or to self-organization of theta oscillations with hippocampal excitation. We also generated difference spectra to capture the percent change of power at each frequency between stationary and running bouts (Fig. 7B). Interestingly, when quantified in this way, behavioral modulation of the theta harmonic was robustly elevated in $Pb^{2+}$-exposed rats relative to controls, whereas behavioral modulation of fundamental theta did not differ significantly between groups. This analysis also revealed a possible reduction of behavioral modulation of relative oscillatory power in the 40-60 Hz range.

*Effect of $Pb^{2+}$ exposure on oscillatory cycle amplitudes.* Our analyses so far have evaluated the spectral content of HC LFPs during stationary and running bouts and have robustly shown that exposure to $Pb^{2+}$ yields marked hypersynchrony and elevated behavioral modulation of the theta rhythm. Our approach has been to compare PSDs directly as well as correlations between power spectra and locomotor behavior. However, these analyses are not well suited to address potential effects of $Pb^{2+}$ on gamma-frequency

synchronization. To evaluate the impact of $Pb^{2+}$ on gamma-frequency synchronization and to further explore delta and theta effects, for each frequency band we compiled the distributions of the peak-to-trough amplitudes of individual cycles during stationary and running bouts (Fig. 8A). As expected, delta, theta, and fast gamma amplitudes were all strongly modulated by behavior for control rats and for $Pb^{2+}$-exposed rats. In contrast, slow gamma did not show differences in amplitude between bout types. Comparisons of $Pb^{2+}$-exposed rats to controls demonstrated pronounced increases in cycle amplitudes for theta- and gamma-frequency bands during stationary bouts (theta: $p=1.4x10^{-236}$, t=-32.9, df=114,635; slow gamma: p=0, t=-78.2, df=554,144; fast gamma: p=0, t=-168.2, df=1,276,491) and during running bouts (theta: p=0, t=-116.5, df=102,653; slow gamma: p=0, t=-90.5, df=491,214; fast gamma: p=0, t=-101.32, df=1,127,377). Although statistically significant, differences in delta cycle amplitudes between $Pb^{2+}$-exposed rats and controls were small relative to those for theta and gamma (stationary: $p=2.9x10^{-8}$, t=-5.5, df=41741; running: $p=1.9x10^{-16}$, t=8.2, df=34211). It is important to consider that with such large numbers of individual cycle amplitude measurements, statistical significance may not be informative.

*Disruption of sensorimotor gating.* In a last series of experiments, we tested the effect of $Pb^{2+}$ exposure on PPI of acoustic startle, an assay of sensorimotor gating known to be impaired in adults with schizophrenia. Figure 8 shows the pattern of results analyzed in males and females across development (PN28, PN50, and PN120). We tested the baseline acoustic startle responses in all groups and found no significant differences (all t-test p's >0.05), suggesting any differences observed in PPI reflect sensory-motor gating.

*Males.* We found effects of Pb2+-exposure in adult males (PN50 and PN120), but not at PN28, demonstrating a developmental trajectory for the emergence of PPI deficits that is similar to schizophrenia. At PN28, a two-way ANOVA showed a main effect of dB level ($F_{2.57, 89.83}$=68.89, p<0.001), no main effect of Pb2+-exposure ($F_{1,35}$ =0.54, p=0.467), and no level x exposure interaction ($F_{2.57, 89.83}$=2.56, p=0.069). At PN50, there was a main effect dB level ($F_{3.12, 109.23}$=53.49, p<0.001), a main effect of Pb2+-exposure ($F_{1,35}$=11.32, p<0.01), but no level x exposure interaction ($F_{3.12, 109.23}$=1.34, p=0.266). At PN120, there was a main effect dB level ($F_{2.88, 115.11}$=59.59, p<0.001), a main effect of Pb2+-exposure ($F_{1,35}$=9.30, p<0.01), but no level x exposure interaction ($F_{2.88, 115.11}$=2.00, p=0.120).

430 *Females.* We found no effects of Pb2+-exposure in female rats at any age. At PN28, a two-way
431 ANOVA showed a main effect of dB level ($F_{2.56, 92.28}$=42.74, p<0.001), no main effect of Pb2+-exposure
432 ($F_{1,36}$ =0.01, p=0.942), and no level x exposure interaction ($F_{2.56, 92.28}$=0.17, p=0.888). At PN50, there was a
433 main effect dB level ($F_{2.89, 101.26}$=90.26, p<0.001), no main effect of Pb2+-exposure ($F_{1,35}$=0.28, p=0.602),
434 and no level x exposure interaction ($F_{2.89, 101.26}$=0.61, p=0.606). At PN120, there was a main effect dB level
435 ($F_{2.82, 104.17}$=57.96, p<0.001), no main effect of Pb2+-exposure ($F_{1,37}$=0.02, p=0.878), and no level x
436 exposure interaction ($F_{2.82, 104.17}$=0.61, p=0.597).
437

438 **Discussion**

439 We analyzed the spectral content of hippocampal LFPs and found that rats chronically exposed to
440 $Pb^{2+}$ exhibited hypersynchrony in the theta- and gamma-frequency bands both while stationary and during
441 running. Behavioral modulation of theta power was also stronger in $Pb^{2+}$-exposed rats relative to controls,
442 suggesting increased efficacy of the neural mechanisms for theta rhythmogenesis as well as elevated
443 baseline levels of theta synchronization. We also found that theta frequency was markedly lower in
444 $Pb^{2+}$-exposed animals than controls, and running speed modulation of theta frequency was restricted to a
445 narrow range of speeds. Thus, chronic $Pb^{2+}$ exposure increased theta synchrony while reducing theta
446 frequency and rendering it less flexible in response to changes in behavior. Slower frequency oscillations
447 are generally associated with synchronization of larger populations of neurons, and intrinsic coupling within
448 hippocampal networks and active membrane properties of hippocampal neurons are well suited to self-
449 organize theta-rhythmic activity (Goutagny et al., 2009, Stark et al., 2015). Importantly, parvalbumin
450 expressing interneurons (PVGIs) are major contributors to theta rhythmic synchronization of hippocampal
451 principal cells (Amilhon et al., 2015), but PVGIs are reduced in animals chronically exposed to $Pb^{2+}$. One
452 potential explanation of this inconsistency is that the reduction in number is compensated for by increased
453 local connectivity of the remaining PVGIs to maintain an appropriate excitatory-inhibitory balance within
454 hippocampal networks. Such a homeostatic function might endow the remaining PVGIs with stronger
455 influence over the spike timing of larger populations of synaptic targets leading to excessive synchrony.
456 Interestingly, ablation of NMDARs on PVGIs (presumably without reducing PVGI number) yields the

opposite pattern of effects on theta than $Pb^{2+}$ exposure, increasing theta frequency while reducing power, and resulting in disrupted hippocampal representations and impaired memory (Korotkova et al., 2010).

In addition to theta hypersynchrony, we also found increased gamma-frequency synchronization in $Pb^{2+}$-exposed animals. Elevated gamma activity in normal animals is integral to cognitive processes including attention, perception, and memory encoding (e.g. Fell et al., 2001, Jutras et al., 2009, Yamamoto et al., 2014, Fries et al., 2001), but $Pb^{2+}$-exposed animals show deficits in cognition and memory. One possibility is that the elevated gamma synchronization seen in $Pb^{2+}$-exposed animals is in fact a consequence of the excessive theta synchrony that we have described. Pastoll and colleagues (2013) showed that theta-frequency excitation of layer II of medial entorhinal cortex *in vitro* was sufficient to elicit well-timed gamma oscillations nested with theta cycles. This demonstrates that the local microcircuitry responsible for gamma synchronization can be engaged by theta-rhythmic excitation in the absence of an intact animal, and this mechanism could be strongly driven by theta hypersynchrony in $Pb^{2+}$-exposed animals.

Importantly, hypersynchrony reflects reduced stochasticity in network dynamics which can be detrimental to encoding capacity and flexibility. We further observed increased behavioral modulation of theta power. It is important to note that this is not behavioral modulation of encoding but rather a greater increase in theta synchronization that could reflect a further decrease in encoding capacity or flexibility during running. For example, single neurons in parahippocampal structures commonly show conjunctive representations of multiple spatial dimensions. When the spatial tuning of conjunctive grid-head direction cells in medial entorhinal cortex is disrupted by inactivation of the medial septum, the fidelity of those cells for head direction tuning is increased (Brandon et al., 2013). Here, we revealed greater fidelity of theta power to running speed, which may also reflect a reduction in the dimensionality of hippocampal encoding. This pattern of effects would be consistent with reduced integration of information types or modalities of sensory input accompanying elevated entrainment of hippocampal populations to theta and stronger encoding fidelity for running speed. This interpretation could also incorporate our finding of disrupted sensorimotor gating resulting from $Pb^{2+}$ exposure. If the hippocampus is excessively involved in encoding behavior, it may be less receptive to incoming sensory information. Furthermore, $Pb^{2+}$ neurotoxicity and

schizophrenia are both related to behavioral inflexibility or cognitive-behavioral perseveration consistent with this general formulation.

Related to the hypersynchrony observed here, $Pb^{2+}$ exposure has been shown to increase the likelihood of epilepsy six-fold (Chang et al., 2011; Clark et al., 2012). Epilepsy is defined by its manifestation of neural hypersynchrony that can be either focal or global. Taking epilepsy as a model, hypersynchrony can cause specific or general cognitive deficits corresponding to focal or global appearances, in addition to the damaging effects of the seizure events on network architecture and dynamics resulting from dysfunctional plasticity resulting from hypersynchrony.

Though a lesser effect, we also note that there were interesting correlations of delta parameters to running speed in Pb2+-exposed rats when delta would normally be expected to be weak (as we previously described, Schultheiss et al., 2020). However, in addition to typical orthogonality between delta- and theta-dominated modes, we sometimes observed apparent correlations between frequency-bands occurring within a given network mode (such as high delta *and* high theta). See Figure 5 insets in Schultheiss et al., (2020). This suggests that $Pb^{2+}$-exposure may also cause atypical cross-frequency couplings that are detrimental to cognition and behavior.

500 **References**

501 Abazyan, B., Dziedzic, J., Hua, K., Abazyan, S., Yang, C., Mori, S., Pletnikov, M. V., & Guilarte, T.
502 R. (2014). Chronic exposure of mutant DISC1 mice to lead produces sex-dependent abnormalities
503 consistent with schizophrenia and related mental disorders: a gene-environment interaction
504 study. *Schizophrenia bulletin*, *40*(3), 575–584. https://doi.org/10.1093/schbul/sbt071

505 Amilhon, B., Huh, C. Y., Manseau, F., Ducharme, G., Nichol, H., Adamantidis, A., & Williams, S.
506 (2015). Parvalbumin Interneurons of Hippocampus Tune Population Activity at Theta Frequency. Neuron,
507 86(5), 1277–1289. https://doi.org/10.1016/j.neuron.2015.05.027

508 Arbab, T., Battaglia, F. P., Pennartz, C., & Bosman, C. A. (2018). Abnormal hippocampal theta and
509 gamma hypersynchrony produces network and spike timing disturbances in the Fmr1-KO mouse model of
510 Fragile X syndrome. *Neurobiology of disease*, *114*, 65–73. https://doi.org/10.1016/j.nbd.2018.02.011

511 Bast, T., Zhang, W. N., & Feldon, J. (2001a). Hyperactivity, decreased startle reactivity, and
512 disrupted prepulse inhibition following disinhibition of the rat ventral hippocampus by the GABA(A) receptor
513 antagonist picrotoxin. *Psychopharmacology*, *156*(2-3), 225–233. https://doi.org/10.1007/s002130100775

514 Bast, T., Zhang, W. N., Heidbreder, C., & Feldon, J. (2001b). Hyperactivity and disruption of
515 prepulse inhibition induced by N-methyl-D-aspartate stimulation of the ventral hippocampus and the effects
516 of pretreatment with haloperidol and clozapine. *Neuroscience*, *103*(2), 325–335.
517 https://doi.org/10.1016/s0306-4522(00)00589-3

518 Bast, T., & Feldon, J. (2003). Hippocampal modulation of sensorimotor processes. *Progress in*
519 *neurobiology*, *70*(4), 319–345. https://doi.org/10.1016/s0301-0082(03)00112-6

520 Brandon, M. P., Bogaard, A. R., Schultheiss, N. W., & Hasselmo, M. E. (2013). Segregation of
521 cortical head direction cell assemblies on alternating θ cycles. Nature neuroscience, 16(6), 739–748.
522 https://doi.org/10.1038/nn.3383

523 Brubaker, C. J., Dietrich, K. N., Lanphear, B. P., & Cecil, K. M. (2010). The influence of age of lead
524 exposure on adult gray matter volume. *Neurotoxicology*, *31*(3), 259–266.
525 https://doi.org/10.1016/j.neuro.2010.03.004

Caito, S., & Aschner, M. (2017). Developmental Neurotoxicity of Lead. *Advances in neurobiology*, *18*, 3–12. https://doi.org/10.1007/978-3-319-60189-2_1

Canfield, R. L., Henderson, C. R., Jr, Cory-Slechta, D. A., Cox, C., Jusko, T. A., & Lanphear, B. P. (2003). Intellectual impairment in children with blood lead concentrations below 10 microg per deciliter. *The New England journal of medicine*, *348*(16), 1517–1526. https://doi.org/10.1056/NEJMoa022848

Cao, X., Huang, S., & Ruan, D. (2008). Enriched environment restores impaired hippocampal long-term potentiation and water maze performance induced by developmental lead exposure in rats. *Developmental psychobiology*, *50*(3), 307–313. https://doi.org/10.1002/dev.20287

Chang, Y. T., Chen, P. C., Tsai, I. J., Sung, F. C., Chin, Z. N., Kuo, H. T., Tsai, C. H., & Chou, I. C. (2011). Bidirectional relation between schizophrenia and epilepsy: a population-based retrospective cohort study. *Epilepsia*, *52*(11), 2036–2042. https://doi.org/10.1111/j.1528-1167.2011.03268.x

Clarke, M. C., Tanskanen, A., Huttunen, M. O., Clancy, M., Cotter, D. R., & Cannon, M. (2012). Evidence for shared susceptibility to epilepsy and psychosis: a population-based family study. *Biological psychiatry*, *71*(9), 836–839. https://doi.org/10.1016/j.biopsych.2012.01.011

Fries, P., Reynolds, J. H., Rorie, A. E., & Desimone, R. (2001). Modulation of oscillatory neuronal synchronization by selective visual attention. *Science* (New York, N.Y.), 291(5508), 1560–1563. https://doi.org/10.1126/science.1055465

Goutagny, R., Jackson, J., & Williams, S. (2009). Self-generated theta oscillations in the hippocampus. *Nature neuroscience*, *12*(12), 1491–1493. https://doi.org/10.1038/nn.2440

Guilarte, T. R., Opler, M., & Pletnikov, M. (2012). Is lead exposure in early life an environmental risk factor for Schizophrenia? Neurobiological connections and testable hypotheses. *Neurotoxicology*, *33*(3), 560–574. https://doi.org/10.1016/j.neuro.2011.11.008

Guilarte T. R. (1997). Pb2+ inhibits NMDA receptor function at high and low affinity sites: developmental and regional brain expression. *Neurotoxicology*, *18*(1), 43–51.

Guilarte, T. R., Miceli, R. C., Altmann, L., Weinsberg, F., Winneke, G., & Wiegand, H. (1993). Chronic prenatal and postnatal Pb2+ exposure increases [3H]MK801 binding sites in adult rat

552 forebrain. *European journal of pharmacology*, *248*(3), 273–275. https://doi.org/10.1016/0926-
553 6917(93)90054-t
554 Guilarte, T. R., & Miceli, R. C. (1992). Age-dependent effects of lead on [3H]MK-801 binding to the
555 NMDA receptor-gated ionophore: in vitro and in vivo studies. *Neuroscience letters*, *148*(1-2), 27–30.
556 https://doi.org/10.1016/0304-3940(92)90796-a
557 Guilarte, T. R., & McGlothan, J. L. (1998). Hippocampal NMDA receptor mRNA undergoes subunit
558 specific changes during developmental lead exposure. *Brain research*, *790*(1-2), 98–107.
559 https://doi.org/10.1016/s0006-8993(98)00054-7
560 Guilarte, T. R., Toscano, C. D., McGlothan, J. L., & Weaver, S. A. (2003). Environmental
561 enrichment reverses cognitive and molecular deficits induced by developmental lead exposure. *Annals of*
562 *neurology*, *53*(1), 50–56. https://doi.org/10.1002/ana.10399
563 Hashimoto, T., Volk, D. W., Eggan, S. M., Mirnics, K., Pierri, J. N., Sun, Z., Sampson, A. R., &
564 Lewis, D. A. (2003). Gene expression deficits in a subclass of GABA neurons in the prefrontal cortex of
565 subjects with schizophrenia. *The Journal of neuroscience : the official journal of the Society for*
566 *Neuroscience*, *23*(15), 6315–6326. https://doi.org/10.1523/JNEUROSCI.23-15-06315.2003
567 Jaako-Movits, K., Zharkovsky, T., Romantchik, O., Jurgenson, M., Merisalu, E., Heidmets, L. T., &
568 Zharkovsky, A. (2005). Developmental lead exposure impairs contextual fear conditioning and reduces
569 adult hippocampal neurogenesis in the rat brain. *International journal of developmental neuroscience : the*
570 *official journal of the International Society for Developmental Neuroscience*, *23*(7), 627–635.
571 https://doi.org/10.1016/j.ijdevneu.2005.07.005
572 Jett, D. A., Kuhlmann, A. C., & Guilarte, T. R. (1997). Intrahippocampal administration of lead (Pb)
573 impairs performance of rats in the Morris water maze. *Pharmacology, biochemistry, and behavior*, *57*(1-2),
574 263–269. https://doi.org/10.1016/s0091-3057(96)00349-8
575 Korotkova, T., Fuchs, E. C., Ponomarenko, A., von Engelhardt, J., & Monyer, H. (2010). NMDA
576 receptor ablation on parvalbumin-positive interneurons impairs hippocampal synchrony, spatial
577 representations, and working memory. Neuron, 68(3), 557–569.
578 https://doi.org/10.1016/j.neuron.2010.09.017

579 Kuhlmann, A. C., McGlothan, J. L., & Guilarte, T. R. (1997). Developmental lead exposure causes
580 spatial learning deficits in adult rats. *Neuroscience letters*, *233*(2-3), 101–104.
581 https://doi.org/10.1016/s0304-3940(97)00633-2
582 McGlothan, J. L., Karcz-Kubicha, M., & Guilarte, T. R. (2008). Developmental lead exposure
583 impairs extinction of conditioned fear in young adult rats. *Neurotoxicology*, *29*(6), 1127–1130.
584 https://doi.org/10.1016/j.neuro.2008.06.010
585 Miranda, M. L., Kim, D., Galeano, M. A., Paul, C. J., Hull, A. P., & Morgan, S. P. (2007). The
586 relationship between early childhood blood lead levels and performance on end-of-grade
587 tests. *Environmental health perspectives*, *115*(8), 1242–1247. https://doi.org/10.1289/ehp.9994
588 Munoz, C., Garbe, K., Lilienthal, H., & Winneke, G. (1988). Significance of hippocampal dysfunction
589 in low level lead exposure of rats. *Neurotoxicology and teratology*, *10*(3), 245–253.
590 https://doi.org/10.1016/0892-0362(88)90024-4
591 Needleman H. L. (1983). Lead at low dose and the behavior of children. *Acta psychiatrica*
592 *Scandinavica. Supplementum*, *303*, 26–37. https://doi.org/10.1111/j.1600-0447.1983.tb00939.x
593 Needleman, H. L., McFarland, C., Ness, R. B., Fienberg, S. E., & Tobin, M. J. (2002). Bone lead
594 levels in adjudicated delinquents. A case control study. *Neurotoxicology and teratology*, *24*(6), 711–717.
595 https://doi.org/10.1016/s0892-0362(02)00269-6
596 Needleman H. (2004). Lead poisoning. *Annual review of medicine*, *55*, 209–222.
597 https://doi.org/10.1146/annurev.med.55.091902.103653
598 Nihei, M. K., Desmond, N. L., McGlothan, J. L., Kuhlmann, A. C., & Guilarte, T. R. (2000). N-methyl-
599 D-aspartate receptor subunit changes are associated with lead-induced deficits of long-term potentiation
600 and spatial learning. *Neuroscience*, *99*(2), 233–242. https://doi.org/10.1016/s0306-4522(00)00192-5
601 Opler, M. G., Brown, A. S., Graziano, J., Desai, M., Zheng, W., Schaefer, C., Factor-Litvak, P., &
602 Susser, E. S. (2004). Prenatal lead exposure, delta-aminolevulinic acid, and schizophrenia. *Environmental*
603 *health perspectives*, *112*(5), 548–552. https://doi.org/10.1289/ehp.6777
604 Opler, M. G., Buka, S. L., Groeger, J., McKeague, I., Wei, C., Factor-Litvak, P., Bresnahan, M.,
605 Graziano, J., Goldstein, J. M., Seidman, L. J., Brown, A. S., & Susser, E. S. (2008). Prenatal exposure to

lead, delta-aminolevulinic acid, and schizophrenia: further evidence. *Environmental health perspectives*, *116*(11), 1586–1590. https://doi.org/10.1289/ehp.10464

Paxinos, G., and Watson, C. (2004). The rat brain in stereotaxic coordinates 5th Edition. (Massachusetts: Academic Press).

Schultheiss, N.W., Schlecht, M., Jayachandran, M., Brooks, D.R., McGlothan, J.L., Guilarte, T.R. & Allen, T.A. (2020). Awake delta and theta-rhythmic hippocampal network modes during intermittent locomotion behaviors in the rat. *Behavioral Neuroscience.*

Stansfield, K. H., Ruby, K. N., Soares, B. D., McGlothan, J. L., Liu, X., & Guilarte, T. R. (2015). Early-life lead exposure recapitulates the selective loss of parvalbumin-positive GABAergic interneurons and subcortical dopamine system hyperactivity present in schizophrenia. *Translational psychiatry*, *5*(3), e522. https://doi.org/10.1038/tp.2014.147

Stark, E., Eichler, R., Roux, L., Fujisawa, S., Rotstein, H. G., & Buzsáki, G. (2013). Inhibition-induced theta resonance in cortical circuits. *Neuron*, *80*(5), 1263–1276. https://doi.org/10.1016/j.neuron.2013.09.033

Wang, T., Guan, R. L., Liu, M. C., Shen, X. F., Chen, J. Y., Zhao, M. G., & Luo, W. J. (2016). Lead Exposure Impairs Hippocampus Related Learning and Memory by Altering Synaptic Plasticity and Morphology During Juvenile Period. *Molecular neurobiology*, *53*(6), 3740–3752. https://doi.org/10.1007/s12035-015-9312-1

Yamamoto J, Suh J, Takeuchi D, Tonegawa S. Successful execution of working memory linked to synchronized high-frequency gamma oscillations. Cell. 2014;157(4):845-857. https://doi:10.1016/j.cell.2014.04.009

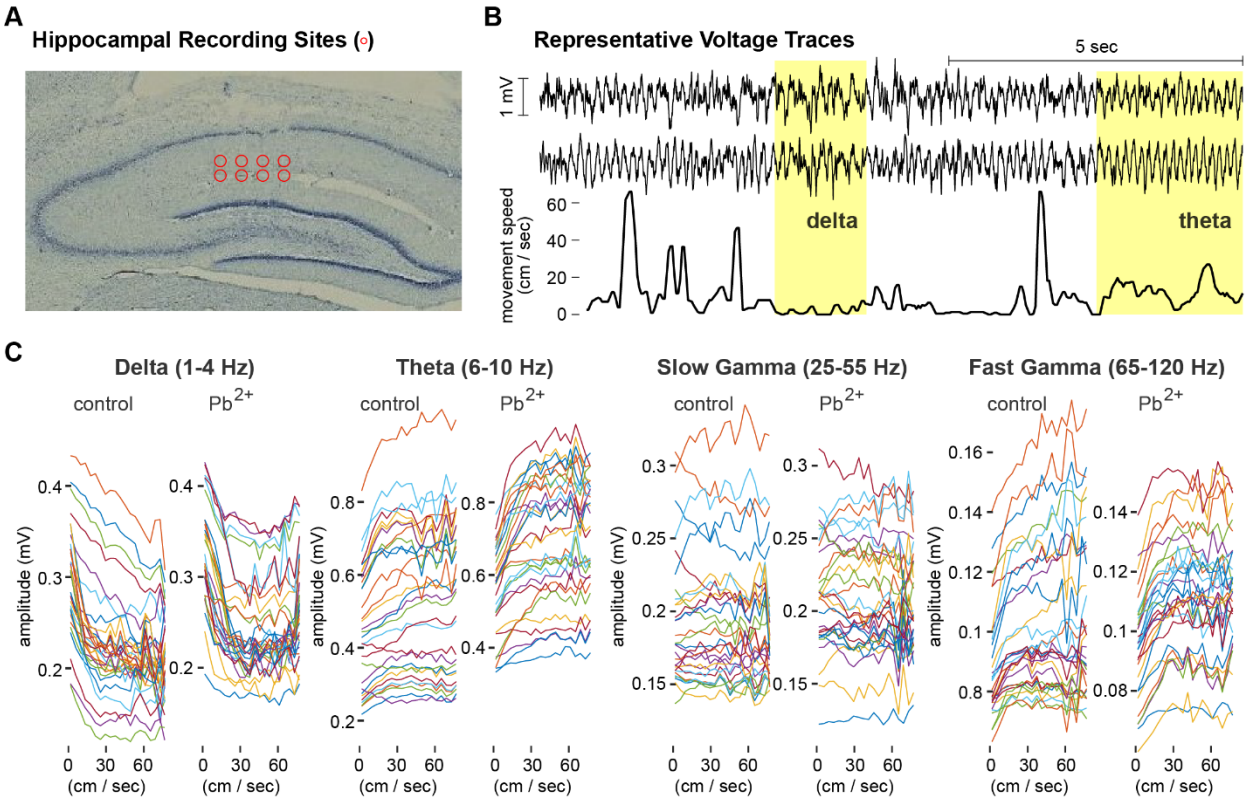


**Figure 1. Movement speed modulation of delta, theta, and gamma oscillations in the hippocampal local field potential (LFP). A.** Eight recording sites (one tetrode each) located at two depths on each of four shanks of a silicon probe. Tracks left by the shanks of the implanted probe are visible as disruptions of the cell layer. **B.** Representative LFP traces recorded while an animal freely explored the behavioral arena (top) and the corresponding movement speed of the animal (bottom). **C.** Movement speed modulation of the amplitudes of delta, theta, and gamma oscillations (across all behaviors) in control rats and rats chronically exposed to lead ($Pb^{2+}$) in their diet.

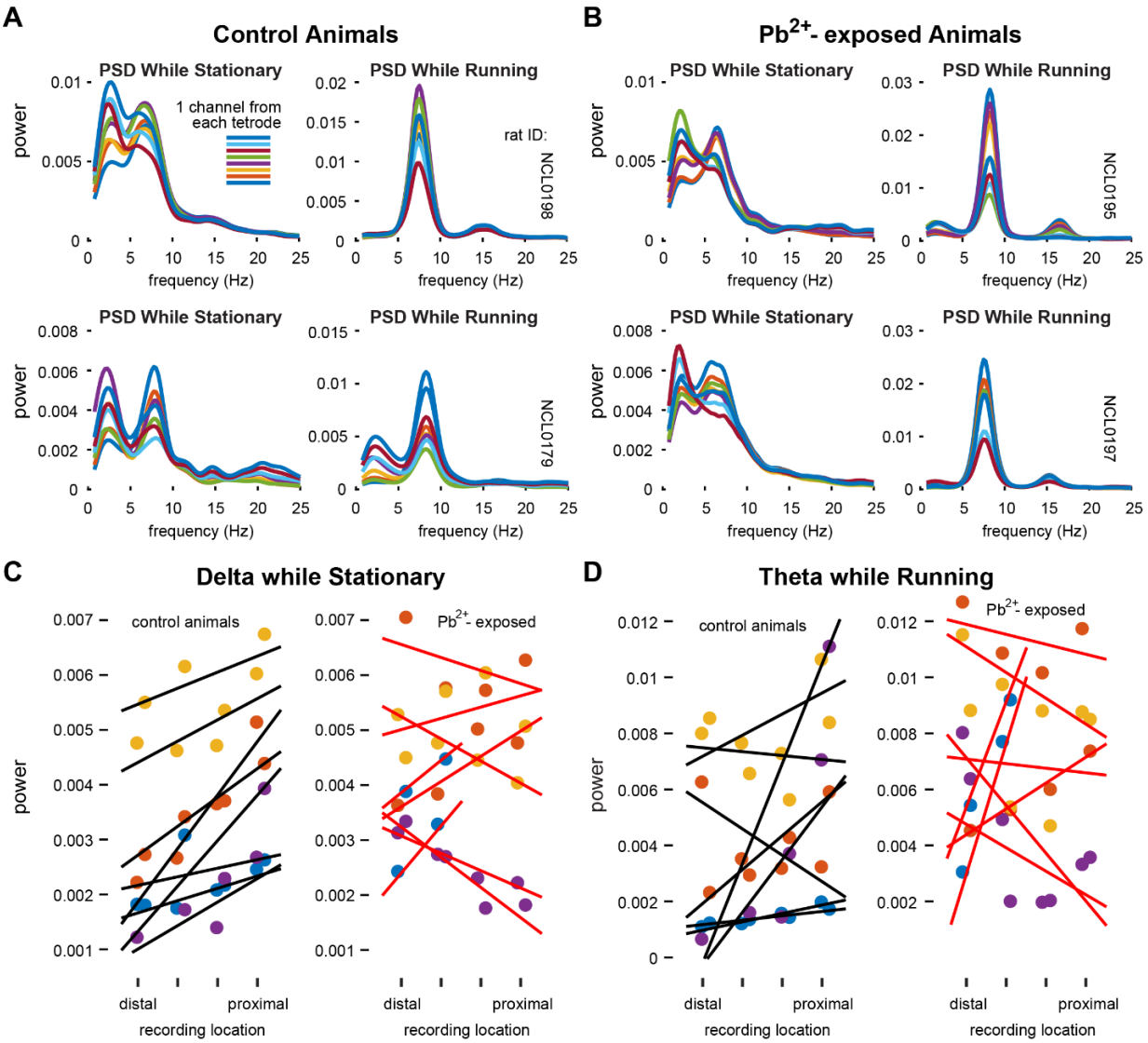


**Figure 2. Power spectra during stationary and running bouts. A.** Diminished delta and heightened theta during running (**right**) relative to stationary bouts (**left**) for two control rats. **B.** As in A for two $Pb^{2+}$-exposed rats. **C.** An apparent proximal-distal gradient in delta power across probe shanks in stationary control animals (**left**), is absent in $Pb^{2+}$-exposed animals (**right**). Black and red lines in C and D reflect the best fits to power estimates along the dorsal and ventral rows of four tetrodes (across shanks) for each rat. **D.** Theta power at sites along the proximal-distal axis in control and $Pb^{2+}$-exposed animals during running bouts.

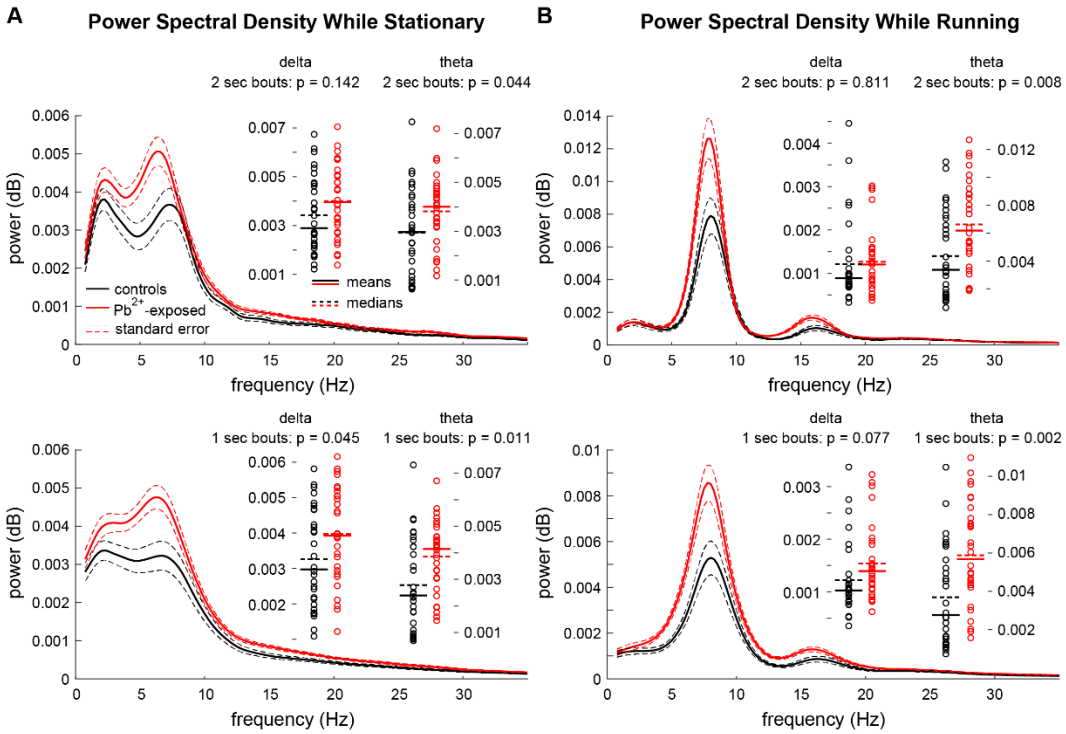


**Figure 3. Theta-frequency hypersynchrony in $Pb^{2+}$-exposed rats. A.** Elevated theta-frequency power in $Pb^{2+}$ rats during stationary bouts (2 sec bouts at **top**, 1 sec bouts **below**). **B.** Marked increase in theta power in $Pb^{2+}$-exposed rats during running bouts.

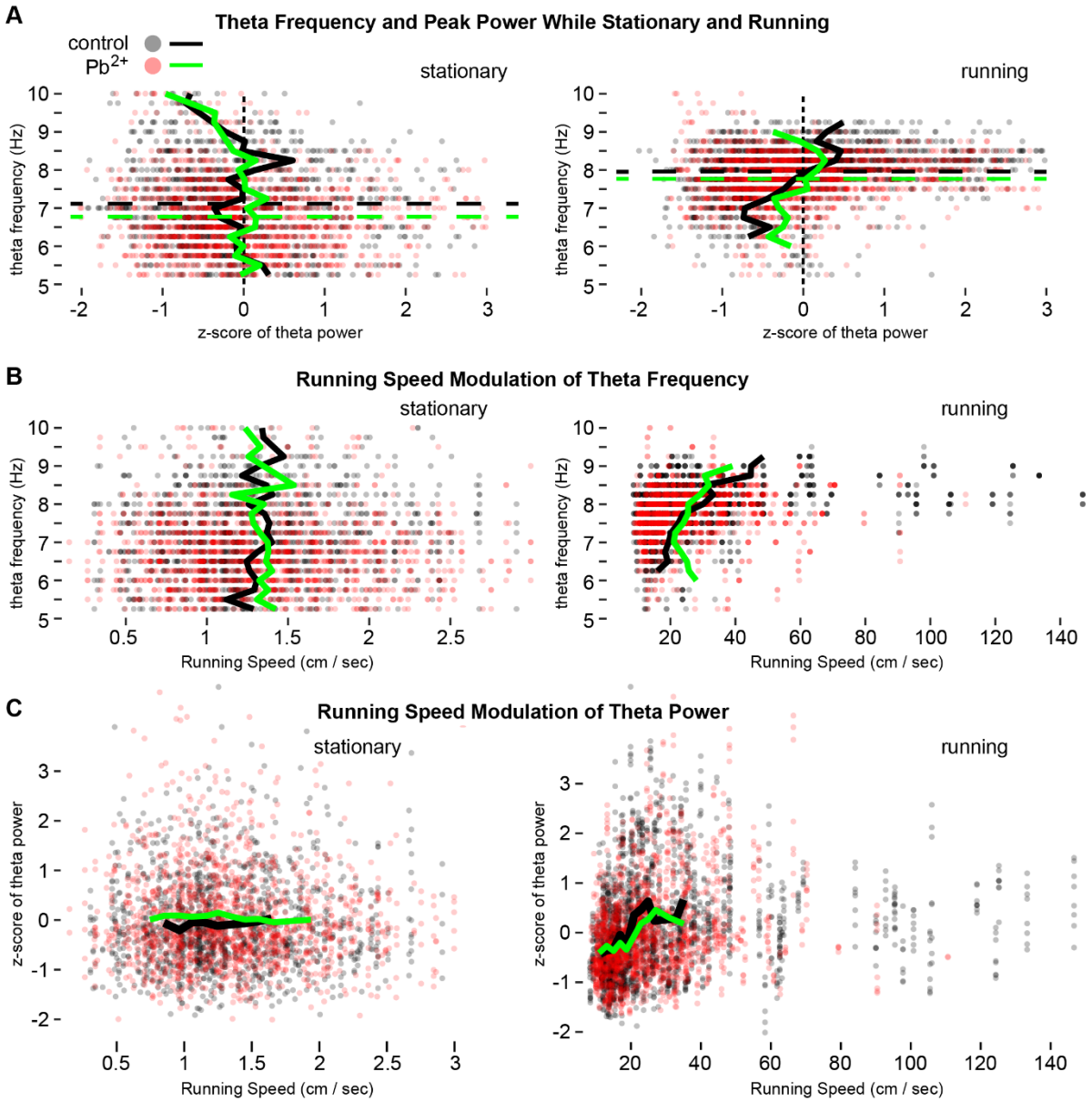


**Figure 4. $Pb^{2+}$ exposure reduces theta frequency and disrupts running speed modulation. A.** Scatter plots of theta power and frequency taken from the power spectral density for each recorded channel during each bout of stationary (**left**) and running behaviors (**right**) for all rats. Black and green lines indicate means for control and $Pb^{2+}$-exposed rats, respectively. Dashed lines indicate the mean theta frequencies for each group. **B.** Running speed modulation of theta frequency. **C.** Running speed modulation of theta power.

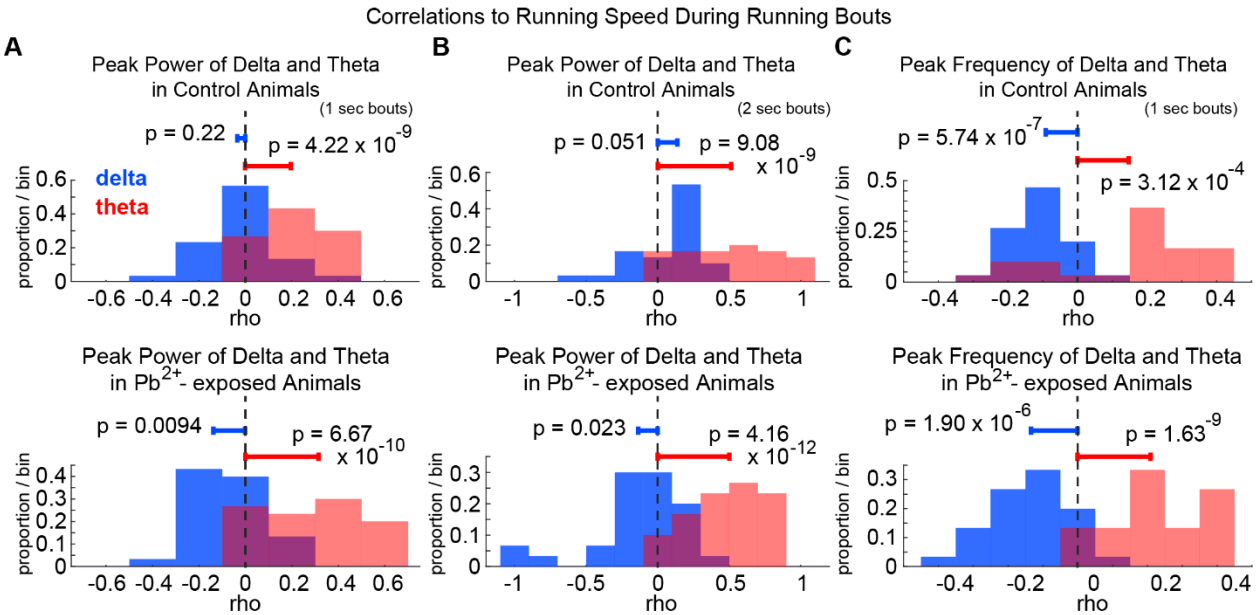


**Figure 5. Running speed modulation of theta power is elevated in $Pb^{2+}$-exposed animals. A.** Distributions of correlation coefficients between delta (blue) and theta (red) power estimates and running speed. Individual correlations were calculated across running bouts (1 sec) for each recorded channel from control rats (**top**) and $Pb^{2+}$-exposed rats (**bottom**). **B.** As in A, for two second running bouts. **C.** As in A, but comparing correlations of delta and theta peak frequencies to running speed.

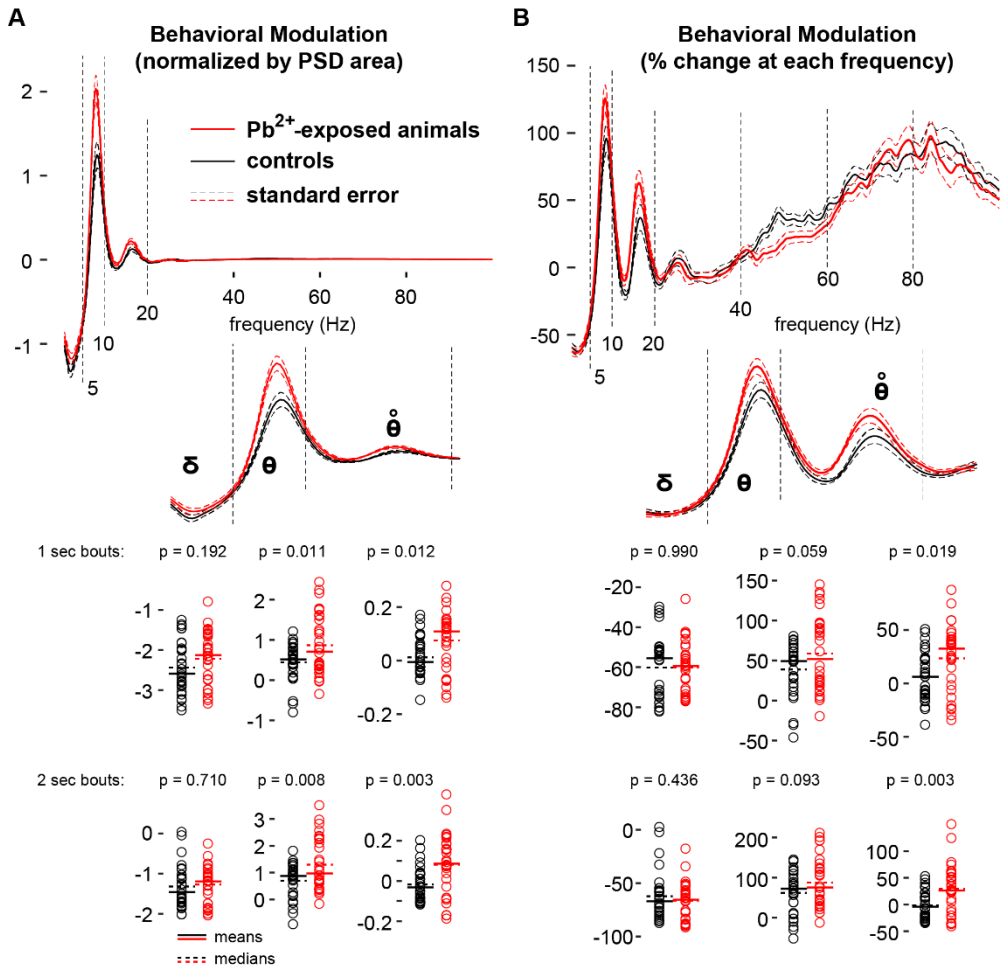


**Figure 6. $Pb^{2+}$-exposure elevates behavioral modulation of theta power. A.** Change in power spectra between stationary and running bouts (**top**) for control (black) and $Pb^{2+}$-exposed rats (red) normalized by total power (0-25 Hz). Enlargement of the low frequency range of PSDs is shown below. Scatters of individual measures for each channel and rat and using one and two second bout definitions (**bottom**). **B.** Percent change in power at each frequency between stationary and running bouts (**top**) for control (black) and $Pb^{2+}$-exposed rats (red). PSD enlargement (**middle**) and scatters (**bottom**) as in A.

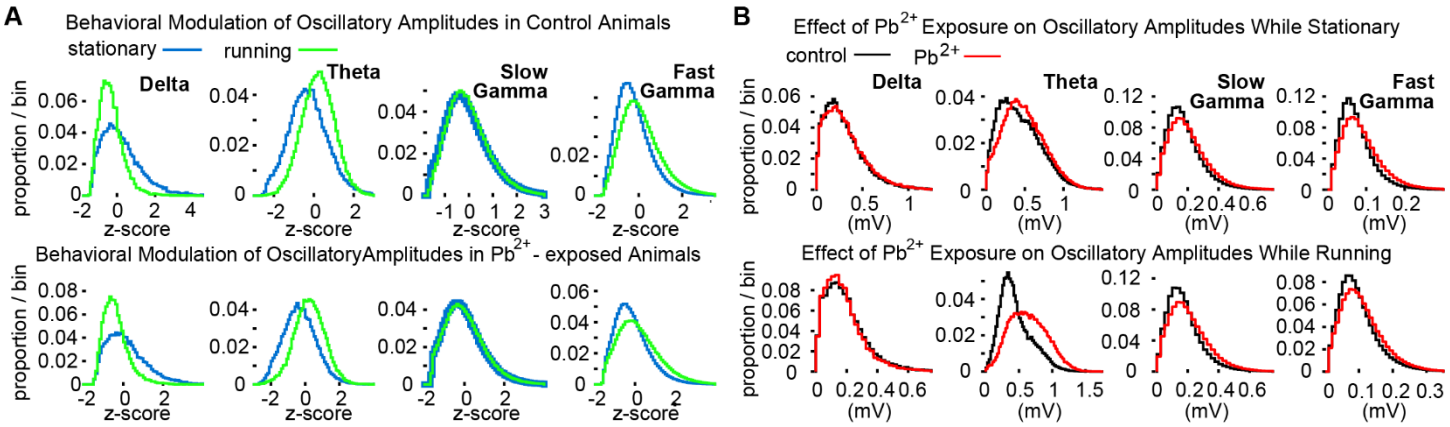


**Figure 7. $Pb^{2+}$ exposure amplifies theta and gamma-frequency synchrony. A.** Distributions of normalized cycle amplitudes for delta, theta, and gamma frequency bands during stationary (blue) and running bouts (green) in control (**top**) and $Pb^{2+}$-exposed animals (**bottom**). **B.** Distributions of unnormalized cycle amplitudes for each frequency band during stationary (**top**) and running bouts (**bottom**) in control (black) and $Pb^{2+}$-exposed animals (red).

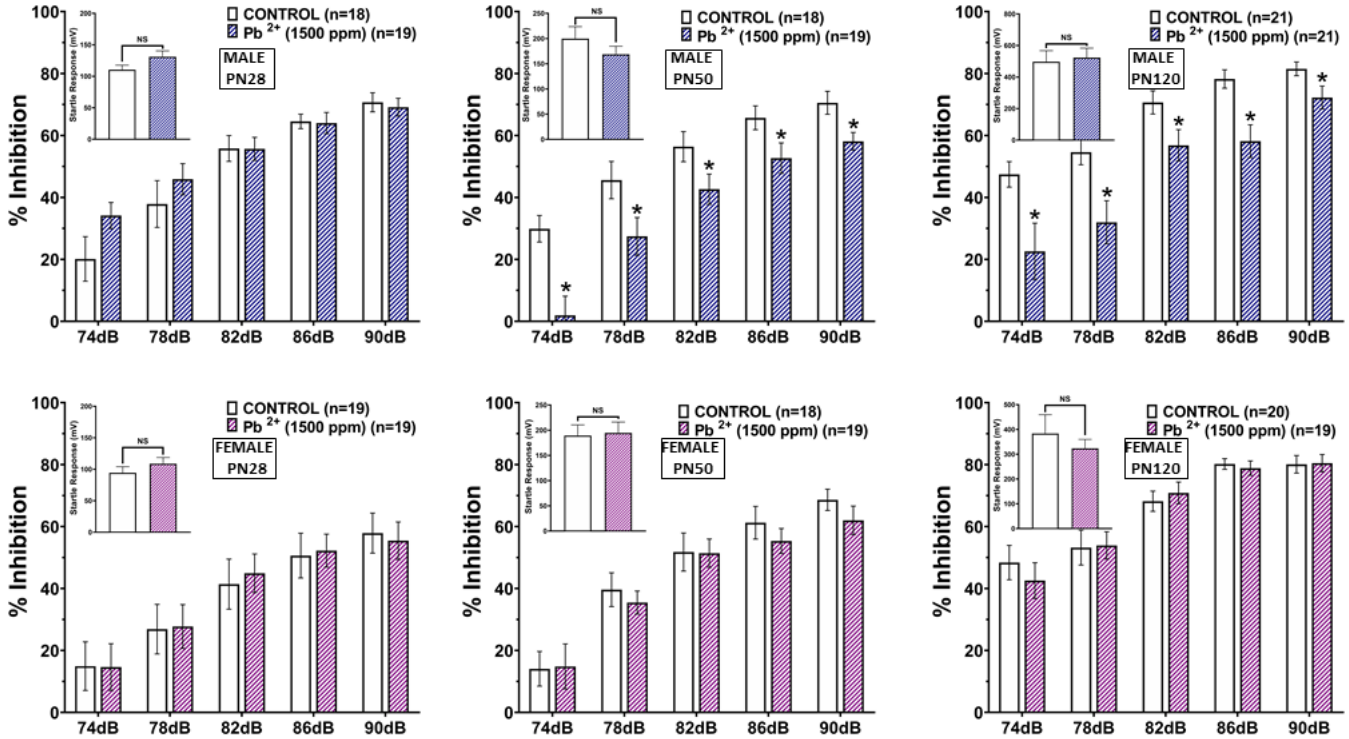


**Figure 8. Prepulse inhibition in male and female rats chronically exposed to $Pb^{2+}$.** The results show no effect of $Pb^{2+}$ exposure at PN28 but marked inhibition of PPI in male rats at PN50 and PN120. No effect of $Pb^{2+}$ exposure was found in female rats at any age. Insert graphs in each panel are startle response at 120 dB. No effect on startle response was observed in $Pb^{2+}$-exposed male or female rats relative to controls at any age. Thus, CELLE does not alter the sensitivity of the animal to a startle. However, CELLE produces a significant deficit on PPI in male rats relative to controls (*$p<0.05$). Data are expressed as mean ± sem. n=number of litters (one male and female animal per litter).

693

| AGE | PN28 | | PN50 | | PN120 | |
|---|---|---|---|---|---|---|
| SEX | Males | Females | Males | Females | Males | Females |
| Control | ≤1.9<br>n=18 | ≤1.9<br>n=16 | ≤1.9<br>n=17 | ≤1.9<br>n=15 | ≤1.9<br>n=17 | ≤1.9<br>n=15 |
| 1500ppm PbAc | 21.1 ± 0.9<br>n=18 | 20.9 ± 1.1<br>n=16 | 20.2 ± 1.1<br>n=17 | 22.1 ± 1.3<br>n=20 | 19.6 ± 1.3<br>n=17 | 24.3 ± 2.2<br>n=14 |
| p-value | ≤0.0001 | ≤0.0001 | ≤0.0001 | ≤0.0001 | ≤0.0001 | ≤0.0001 |

694

695 **Table 1:** Blood $Pb^{2+}$ levels (μg/dL) in male and female rats contributing to data represented in Figure 9. Each
696 value is the mean ± sem. n= number of litters (one male and female animal per litter).
697

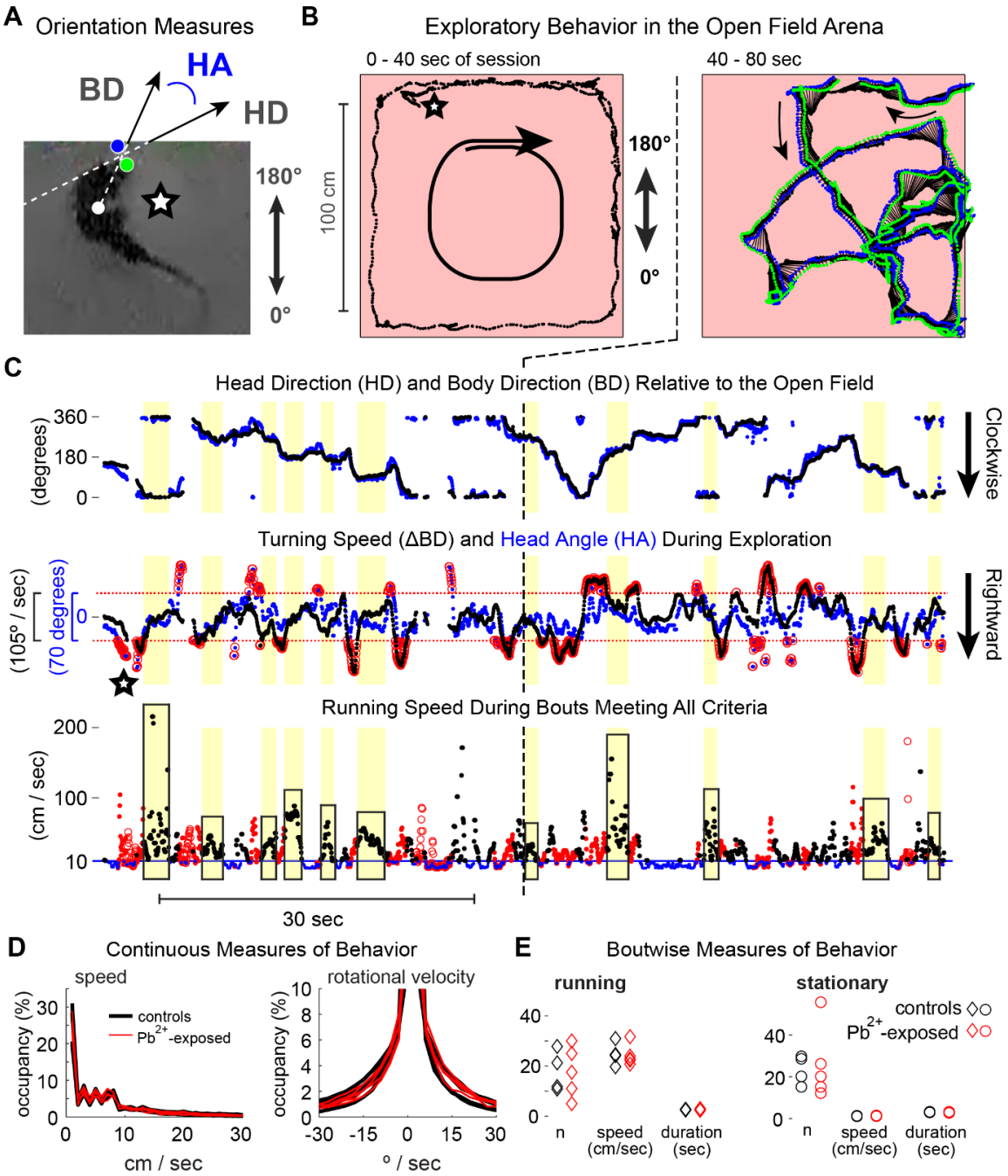


**Supplemental Figure 1. Precise delineation of stationary and running bouts. A.** Schematic of the orientation measures used in definitions of behavioral bouts. The star indicates the rat's location in B when the image was captured. **B.** Representative locomotor trajectories showing thigmotaxis during the first 40 seconds of an experimental session (**left**) followed by runs through the interior of the open field arena during the subsequent epoch (**right**). Arrows indicate the rat's direction of running. As in A, blue and green points represent head-mounted LEDs used to derive orientation measures, and black line segments capture the rat's body orientation at each timepoint. **C.** Head and body direction (**top**) were used to derive rotational velocity and head angle (**middle**), which in turn were used to identify bouts of running (**bottom**) while excluding rotational and reorienting behaviors (red points and circles). **D.** Speed occupancy (**left**) and rotational velocity (**right**) measured throughout behavioral sessions did not differ between control and $Pb^{2+}$-exposed rats, nor did bout-wise behavioral measures (**F**) of running (**left**) and stationary bouts (**right**), including the numbers of bouts, median movement speeds, and bout durations.